SCIENTIFIC REPORTS

OPEN

Li(Cd,Mn)P: a new cadmium based diluted ferromagnetic semiconductor with independent spin & charge doping

Received: 26 June 2018
Accepted: 13 December 2018
Published online: 16 May 2019

W. Han[1,2,3], B. J. Chen[1,2], B. Gu[4,5], G. Q. Zhao[1,2], S. Yu[1,2], X. C. Wang[1,2], Q. Q. Liu[1,2], Z. Deng[1,2], W. M. Li[1,2], J. F. Zhao[1,2], L. P. Cao[1,2], Y. Peng[1,6], X. Shen[1], X. H. Zhu[6], R. C. Yu[1], S. Maekawa[5], Y. J. Uemura[7] & C. Q. Jin[1,2,8]

We report a new diluted ferromagnetic semiconductor Li_{1+y}(Cd,Mn)P, wherein carrier is doped via excess Li while spin is doped by isovalence substitution of Mn^{2+} into Cd^{2+}. The extended Cd 4*d*-orbitals lead to more itinerant characters of Li_{1+y}(Cd,Mn)P than that of analogous Li_{1+y}(Zn,Mn)P. A higher Curie temperature of 45 K than that for Li_{1+y}(Zn,Mn)P is obtained in Li_{1+y}(Cd,Mn)P polycrystalline samples by Arrott plot technique. The p-type carriers are determined by Hall effect measurements. The first principle calculations and X-ray diffraction measurements indicate that occupation of excess Li is at Cd sites rather than the interstitial site. Consequently holes are doped by excess Li substitution. More interestingly Li_{1+y}(Cd,Mn)P shows a very low coercive field (<100 Oe) and giant negative magnetoresistance (~80%) in ferromagnetic state that will benefit potential spintronics applications.

Diluted ferromagnetic semiconductors have received extensive attention because of their potential applications for spintronics devices[1–3]. For the prototypical III-V diluted ferromagnetic semiconductors, such as (Ga,Mn)As, substitution of divalent Mn^{2+} into trivalent Ga^{3+} results in coupled spin & charge doping, which makes individual control of spin and charge difficult[4]. Additionally, the heterovalent substitution of Mn^{2+} into Ga^{3+} also leads to severely limited chemical solubility, and results in the specimens only available as thin films and sensitive to preparation methods and annealing treatments[5,6]. The coupled spin and charge is an obstacle not only for fundamental understanding of ferromagnetic mechanism but also for effective improvement of controllable Curie temperature (T_C).

Recently a series of new generation diluted ferromagnetic semiconductors, *e.g.* "111" type Li(Zn,Mn)As and Li(Zn,Mn)P, "122" type (Ba,K)(Zn,Mn)$_2$As$_2$ and "1111" type (La,Ca)(Zn,Mn)SbO, have been discovered to overcome the aforementioned difficulties[7–16]. In these new types of diluted ferromagnetic semiconductors spin is doped via isovalent substitution of (Zn^{2+},Mn^{2+}), while charge is provided by off-stoichiometry of Li in the "111" type diluted ferromagnetic semiconductors or by heterovalent substitution of cations in the "122" and "1111" diluted ferromagnetic semiconductors. With the advantage of independent spin and charge doping, a record of controllable T_C of 230 K is achieved in (Ba,K)(Zn,Mn)$_2$As$_2$[10,17]. Furthermore, a number of progresses of these new generation diluted ferromagnetic semiconductors have been made on both fundamental studies and potential applications[18–22]. Large size single crystals and single-phase thin films of (Ba,K)(Zn,Mn)$_2$As$_2$ have been grown[23–25]. Based on single crystal samples, a Mn-impurity band is identified by angle-resolved resonance photoemission spectroscopy, demonstrating strong hybridization between Mn 3*d*- and As 4*p*-orbitals[26]. The magnetic pair distribution function measurements discover presence of robust nearest-neighbor ferromagnetic alignment of Mn spins along the *c* axis even well above T_C[27]. Andreev reflection junction is fabricated with single crystal (Ba,K)

[1]Beijing National Laboratory for Condensed Matter Physics, and Institute of Physics, Chinese Academy of Sciences, Beijing, 100190, China. [2]School of Physics, University of Chinese Academy of Sciences, Beijing, 100190, China. [3]Department of Physics and Electronic Engineering, Hebei Normal University for Nationalities, Chengde, 067000, China. [4]Kavli Institute for Theoretical Sciences & CAS Center for Excellence in Topological Quantum Computation, University of Chinese Academy of Sciences, Beijing, 100190, China. [5]Advanced Science Research Center, Japan Atomic Energy Agency, Tokai, 319-1195, Japan. [6]Department of Materials Science & Engineering, Sichuan University, Chengdu, China. [7]Department of Physics, Columbia University, New York, New York, 10027, USA. [8]Songshan Lake Materials Laboratory, Dongguan, Guangdong, 523808, China. Correspondence and requests for materials should be addressed to Z.D. (email: dengzheng@iphy.ac.cn) or C.Q.J. (email: Jin@iphy.ac.cn)

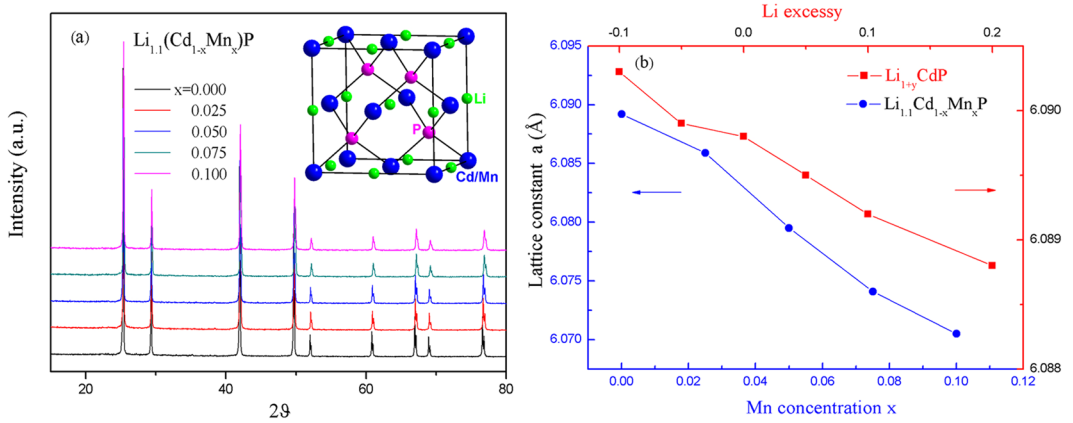

Figure 1. The structure characterizations. (**a**) Powder XRD patterns of $Li_{1.1}(Cd_{1-x}Mn_x)P$ with various Mn, inset: crystal structures of cubic LiCdP. (**b**) Lattice constant of $Li_{1.1}(Cd_{1-x}Mn_x)P$ (blue symbols, bottom horizontal axis) and $Li_{1+y}CdP$ (red symbols, top horizontal axis).

$(Zn,Mn)_2As_2$. The obtained spin polarization rate of 66% is comparable to the prototypical diluted ferromagnetic semiconductors, suggesting large potentials of application in these new generation diluted ferromagnetic semiconductors[28–30].

Improvement of T_C is always a fundamental issue for diluted ferromagnetic semiconductor materials. As well known, T_C depends on the *p-d* exchange between carriers and Mn ions. Generally, greater *p-d* exchange can be reached by shortening bond length in Mn-ligand. However among the "111" diluted ferromagnetic semiconductor materials, Li(Zn,Mn)P has lower hole concentration and lower T_C than those of Li(Zn,Mn)As. Generally, ferromagnetism in a diluted magnetic semiconductor is mediated by itinerated carriers. Thus a higher T_C is expected with further carrier doping in Li(Zn,Mn)P. However, further improvement of carrier concentration by changing the Li concentration is invalid in Li(Zn,Mn)P. To overcome the difficulty we make a new diluted ferromagnetic semiconductor compound Li(Cd,Mn)P, where the extended Cd 4*d*-orbitals lead to more itinerant characters of Li(Cd,Mn)P than that of analogous Li(Zn,Mn)P. Li(Cd,Mn)P is expected to have larger hole concentration and consequently higher T_C than Li(Zn,Mn)P. In this article we report the synthesis and characterizations of the Cd-based diluted ferromagnetic semiconductor, Li(Cd,Mn)P.

Results and Discussion

Crystal structure. Figure 1(a) shows powder X-ray diffraction (XRD) patterns for the samples $Li_{1.1}(Cd_{1-x}Mn_x)P$ (x = 0.025, 0.05, 0.075 and 0.1). Parent phase LiCdP and doped samples Li(CdMn)P crystallize into a zinc-blende like structure with the space group of *F*-43*m*, as shown in the inset of Fig. 1(a). The lattice parameter $a = 6.089(2)$ Å for parent phase LiCdP is consistent with the previous report[31] and larger than LiZnAs ($a = 5.940(2)$ Å) and LiZnP ($a = 5.756(1)$ Å).

Homogeneity and real atomic ratios are studied with energy dispersive analysis (EDX). Except the light element Li, the atomic ratios of Cd, Mn and P are measured. The results show that all the detected elements are well distributed and their ratios are consistent with the nominal compositions (see Supplementary Fig. S1 and Tables S1 and S2). Thus the nominal compositions are used in this article for simplification. The high resolution transmission electron microscope (TEM) measurements were performed on a typical sample, the heaviest doped sample $Li_{1.1}Cd_{0.9}Mn_{0.1}P$. The results don't show any trace of defect or cluster (Fig. S3). The changes of lattice parameters with varying Li and Mn concentration in $Li_{1+y}(Cd_{1-x}Mn_x)P$ are shown in Fig. 1(b). The monotonic changes of lattice parameter with increasing Li and Mn suggest successful chemical doping. The lattice shrinks with Mn substitution due to smaller radius of Mn^{2+} (0.66 Å) than that of Cd^{2+} (0.78 Å)[32]. The decrease of lattice parameter with increasing Li concentration will be discussed later.

Magnetic properties. Parent phase LiCdP is diamagnetic. Single excess Li- and Mn-doping just makes the compound Pauli paramagnetic and paramagnetic (see Supplementary Fig. S2). Ferromagnetism emerges only in Li and Mn co-doped compounds in which excess Li and (Zn,Mn) substitution provide carrier and spin, respectively. The temperature dependence of magnetization ($M(T)$)for $Li_{1.1}(Cd_{1-x}Mn_x)P$ present upturns on lowering temperature, clear signatures of ferromagnetic transition, as shown in Fig. 2(a). Note that no visible difference is detected between field cooling (FC) and zero field cooling (ZFC) modes. Among all possible impurities, only Mn_3O_4 has a comparable $T_C = 42$ K. In contrary, T_C of Li(Cd,Mn)P compounds changes from 15 K to 45 K according to their composition, ruling out the possibility of Mn_3O_4. The hysteresis curve ($M(H)$)of $Li_{1.1}(Cd_{0.925}Mn_{0.075})P$ at $T = 6$ K is plotted in Fig. 2(b) as a typical example. It exhibits ferromagnetic behavior with a small linear field-dependent component, which should be due to remaining paramagnetic spins[9]. Because Mn cations are randomly distributed in material, some Mn cations which locate far away from each other cannot be mediated by carries to form long range ferromagnetic order and consequently lead to local paramagnetic spins. The inset of Fig. 2(b) shows a small coercive field ($H_C < 100$ Oe) that is promising for spin manipulation. After subtracting the linear field-dependent component, the magnetic hysteresis loops of $Li_{1.1}(Cd_{1-x}Mn_x)P$ (x = 0.025, 0.05, 0.075 and 0.10) specimens at 6 K are shown in Fig. 2(c). Because the magnetizations doesn't saturate even up to 1 T, after

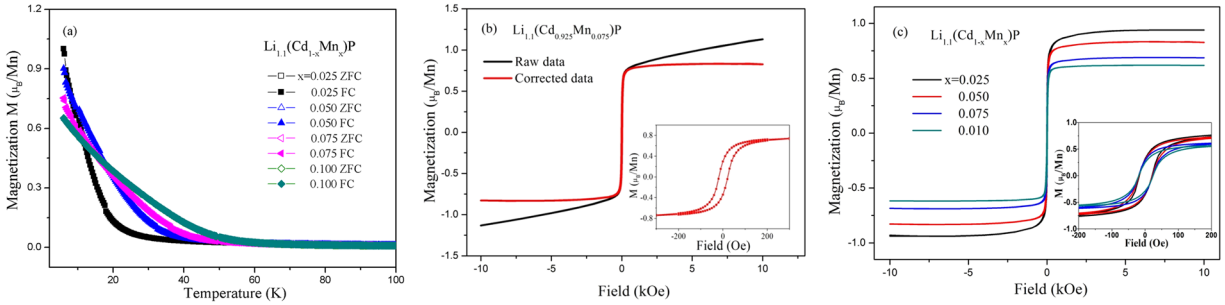

Figure 2. Magnetism of $Li_{1.1}(Cd_{1-x}Mn_x)P$ with x = 0.025–0.10. (**a**) M(T) under applied field H = 2 kOe with ZFC and FC procedures. (**b**) M(H) of $Li_{1.1}(Cd_{0.925}Mn_{0.075})P$ at T = 6 K, measured under applied field H up to 1 T, showing hysteresis loop before and after subtraction of linear field-dependent component. Inset: hysteresis in small field regions. (**c**) M(H) curves after subtraction of the field-dependent component of $Li_{1.1}(Cd_{1-x}Mn_x)P$ with x = 0.025–0.10. Inset: corresponding M(H) curves in small field regions.

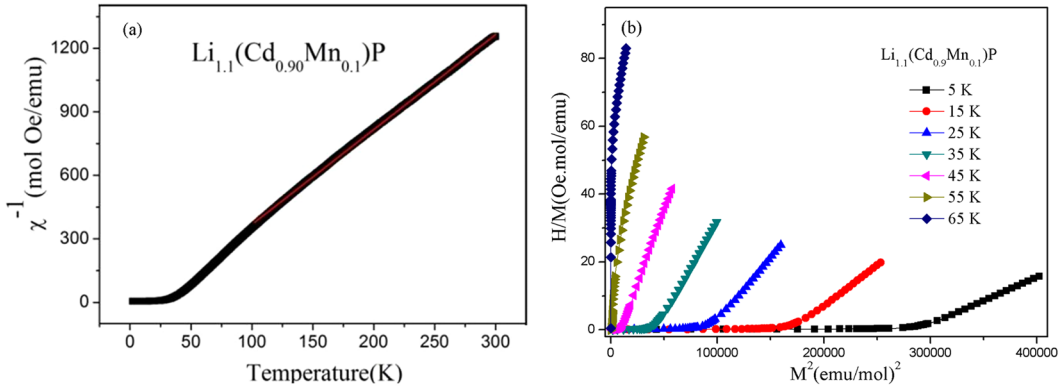

Figure 3. The ferromagnetic ordered temperature of the diluted magnetic semiconductor. (**a**) Inverse susceptibility dependence of temperature for $Li_{1.1}(Cd_{0.9}Mn_{0.1})P$ (black line) and Curie-Weiss fit (red line). (**b**) Arrott plots at various temperatures above and below Tc for $Li_{1.1}(Cd_{0.9}Mn_{0.1})P$, shows the ferromagnetic transition at Tc = 45 K.

subtraction the magnetizations at 6 K and 1 T ($M_{6K,1T}$) is used to approximately represent saturation magnetizations in following discussions. The $M_{6K,1T}$ = 0.94, 0.83, 0.69, 0.62 μ_B/Mn for samples of x = 0.025, 0.05, 0.075 and 0.10 respectively. They are smaller than that of (Ga,Mn)As[4] and Li(Zn,Mn)As[7] possibly due to the competition between the long range ferromagnetic ordering and the short range antiferromagtic interactions. The tendency that the $M_{6K,1T}$ reduces with increasing Mn doping levels has also been found in many magnetic ions doped materials[33]. One rational reason is the competition between ferromagnetic interaction of Mn mediated by carriers and antiferromagnetic coupling of Mn pairs in the nearest neighbor sites, as discussed in "111" and "122" diluted ferromagnetic semiconductors[7–9,12].

In the paramagnetic region, the susceptibility can be well fitted by the Curie-Weiss law, as shown in Fig. 3(a). The obtained Weiss temperature is 17.8(2) K, demonstrating the ferromagnetic interaction between Mn. To precisely determine the T_C, Arrott plot method is performed. In Fig. 3(b), H/M versus M^2 is plotted over the temperature range of 5–65 K. The isotherm at the Curie point is supposed to be a straight line passing through the origin. In this way, T_C is determined as 45 K for $Li_{1.1}(Cd_{0.9}Mn_{0.1})P$. The T_C for the other samples are obtained in similar way. Table 1 lists T_C and $M_{6K,1T}$ for various compositions of $Li_{1+y}(Cd_{1-x}Mn_x)P$. When Mn concentration is fixed, one can note that excess Li initially improves both T_C and $M_{6K,1T}$ within low Li concentration but then suppresses ferromagnetic order when y = 0.2. On the other hand, except samples with overdoped Li (y = 0.2), increasing Mn enhances the T_C but declines the average local moments on Mn ($M_{6K,1T}$).

Electrical transport properties. Figure 4(a) shows the temperature-dependent resistivity ($\rho(T)$) for a series of $Li_{1+y}CdP$ (y = 0, 0.05 and 0.1). Consistent with ref.[31], the parent compound LiCdP present semiconducting conduction[31]. Excess Li doping decrease resistivity, suggesting the effective doping of carriers. Figure 4(b) shows that at the entire temperature range the resistivity of $Li_{1.1}(Cd_{1-x}Mn_x)P$ increases with increasing Mn concentration, caused by localization effect. Although carriers introduced by excess Li doping are originally itinerant, they will be weakly bound to the Mn local spin moments and then partially lose their mobility[34]. The similar conducting behavior has been observed in $(Ba,K)(Zn,Mn)_2As_2$. The localization of the carriers has been confirmed by Mn $K\beta$ x-ray emission spectroscopy measurements which indicates that Mn local spin moments traps holes and in turn is declined by hole doping[20].

T_C (K)/$M_{6K,1T}$ (μ_B/Mn)	y = 0.05	y = 0.1	y = 0.2
x = 0.025	23/0.84	21/0.94	15/0.71
x = 0.05	27/0.72	27/0.83	16/0.37
x = 0.075	31/0.60	35/0.69	16/0.18
x = 0.10	36/0.56	45/0.62	15/0.26

Table 1. The Curie temperature (T_C) and $M_{6K,1T}$ to approximately represent saturation magnetizations of $Li_{1+y}(Cd_{1-x}Mn_x)P$.

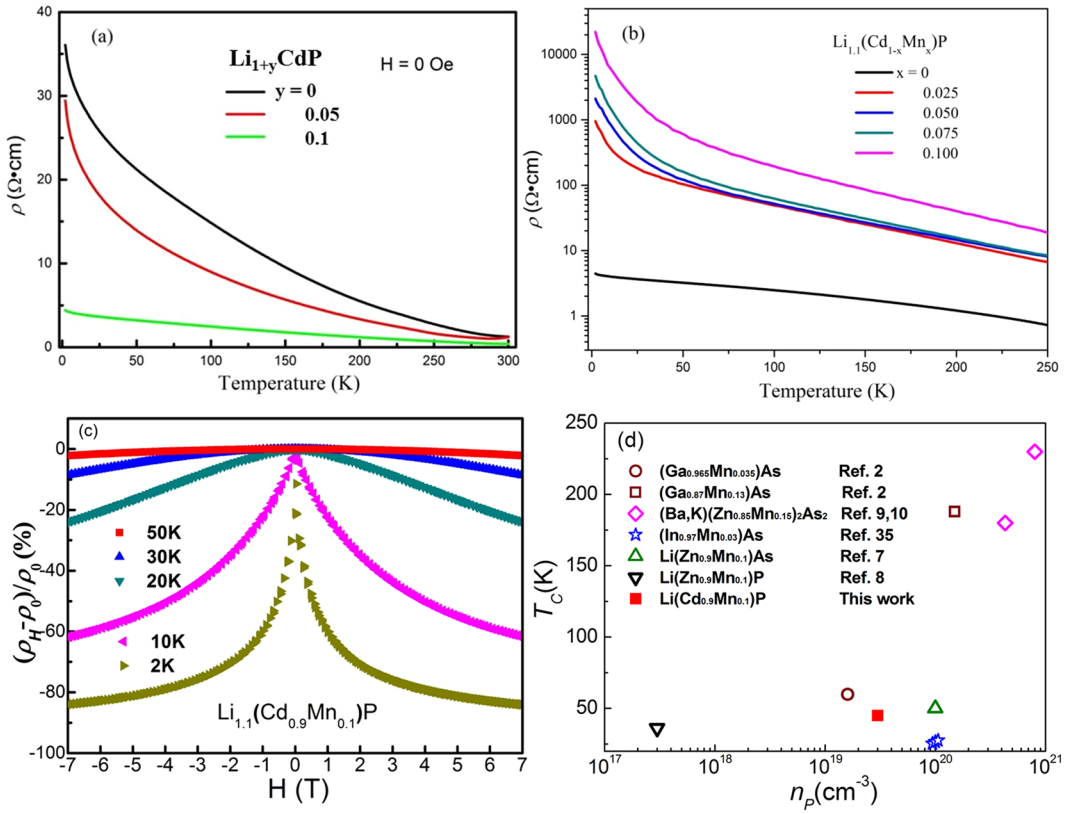

Figure 4. Transport properties of $Li_{1+y}(Cd_{1-x}Mn_x)P$: (**a**) ρ(T) of $Li_{1+y}CdP$ with y = 0, 0.05 and 0.1. (**b**) ρ(T) of $Li_{1.1}(Cd_{1-x}Mn_x)P$ with x = 0, 0.025, 0.05, 0.075 and 0.1. (**c**) Magnetoresistance of $Li_{1.1}(Cd_{0.9}Mn_{0.1})P$ at different temperatures. (**d**) Correlation between T_C and the hole concentration for several "111", "122" new types of diluted ferromagnetic semiconductors and typical III-V diluted ferromagnetic semiconductors.

A giant negative magnetoresistance (MR) is observed in all of the ferromagnetic Li(CdMn)P samples. Figure 4(c) shows the MR of $Li_{1.1}(Cd_{0.9}Mn_{0.1})P$ specimen as a typical example. The value of negative MR (about −80%) is at least twice larger than those of analogues Li(Zn,Mn)As and Li(Zn,Mn)P[7,8]. The negative MR may result from reduction of spin-dependent scattering by aligning the spins under applied field. The Hall effect measurements of all the samples show p-type carriers. Hole concentration (n_p) of the parent phase is ~10^{17} cm^{-3} at 200 K. More holes are doped by excess Li substitution in $Li_{1.1}CdP$ which has $n_p = 3.8 \times 10^{19}$ cm^{-3} at 200 K. In ferromagnetic sample $Li_{1.1}(Cd_{0.95}Mn_{0.05})P$, 5% Mn doping slightly decreases to $n_p = 2.7 \times 10^{19}$ cm^{-3} at 200 K. At lower temperature the resistivity was too large, any small misalignment of the two Hall contacts picks up a longitudinal resistivity signal and this leads to great difficulty in the Hall effect measurement (see Supplementary Fig. S4). The relationships between hole concentration and Curie temperature of "111" diluted ferromagnetic semiconductors and other diluted ferromagnetic semiconductor systems are plotted in Fig. 4(d)[2,7–10,35]. From Li(Zn,Mn)P to Li(Cd,Mn)P, the hole concentration is considerably increased, and consequently the T_C is improved from 34 K to 45 K. As the Zener model predicted, the ferromagnetism is mediated by carriers, and the Curie temperature is positive correlated with hole concentration.

Theoretical analysis. In order to have insight into the origin of hole carrier, we performed calculation on electronic structures with density functional theory (DFT). Calculation shows that the band structure of LiCdP is very similar to that of LiZnP. The band structure of parent phase LiCdP is shown in Fig. S5. The obtained direct energy gap is 0.59 eV. With the quantum Monte Carlo (QMC) simulation of the Anderson impurity model, the impurity band level of Mn is determined as −0.35 eV.

LiCdP with excess Li	Formation energy (Li-rich and Cd-rich limit)	Formation energy (Li-rich and P-rich limit)
Interstitial Li (supercell $Li_{28}Cd_{27}P_{27}$)	2.13 eV	2.13 eV
Li at Cd site and Cd is removed (supercell $Li_{28}Cd_{26}P_{27}$)	0.22 eV	−1.14 eV

Table 2. Formation energy for excess Li atom at different sites, obtained by DFT calculations[36].

Two possible different sites for excess Li are discussed in the calculations, (i) the interstitial site Li_I and (ii) the Cd-substitutional site Li_{Cd}. The former can provide n-type carrier and the latter will serve as a hole donor. We calculate the formation energy for the two excess Li-sites, respectively. Since Mn at Cd-substitutional site Mn_{Cd} does not introduce any carriers, we study the excess Li in $Li_{1+y}CdP$ for simplification. According to previous work[36], the formation energy is given by $E_{formation} = E_T - n_{Li}\mu_{Li} - n_{Cd}\mu_{Cd} - n_P\mu_P$, where E_T is the total energy of the supercell, n_x is the number of x atoms in the supercell, and μ_x is the atomic chemical potential. It has $\mu_{Li} + \mu_{Cd} + \mu_P = \mu_{LiCdP(bulk)}$. Table 2 shows formation energy for two extreme conditions, *i.e.*, the Li-rich plus Cd-rich limit ($\mu_{Li} = \mu_{Li(bulk)}$, $\mu_{Cd} = \mu_{Cd(bulk)}$) and the Li-rich plus P-rich limit ($\mu_{Li} = \mu_{Li(bulk)}$, $\mu_P = \mu_{P(bulk,black)}$). Under both conditions, compounds with Li_{Cd} have lower formation energy. The experimental condition must be between these two extreme conditions. It recalls the reduction of lattice parameter with excess Li doping found in XRD measurements. The excess Li at interstitial site is supposed to stretch the lattice. In contrary, substitution of Li into Cd should shrink the lattice due to the smaller Li^+ radius (0.59 Å) than Cd^{2+} (0.78 Å)[32]. Thus we argue that in Li(Cd,Mn)P the excess Li atoms prefer to occupy Cd-substitutional sites Li_{Cd}, and thus create the p-type carriers.

Conclusions

In this work, "111" type Cd-based Li(Cd,Mn)P has been designed to achieve high Curie temperature. In Li(Cd,Mn)P replacement of Zn by Cd successfully compensates for the high hole binding energy in the Li(Zn,Mn)P by increasing Mn-P bond length. As a result, Li(Cd,Mn)P has enlarged the hole concentration, amplified the effective *p-d* exchange and more importantly a Curie temperature of 45 K which is one third higher than T_C of Li(Zn,Mn)P. In addition, the observed properties in Li(Cd,Mn)P, such as the low coercive field and the giant negative magnetoresistance, are favorable for future applications. In short, the successful prediction and fabrication of Li(Cd,Mn)P open an new boulevard to tailor the ferromagnetism in diluted magnetic semiconductors.

Method

Polycrystalline specimens of Li(Cd,Mn)P were prepared by solid state reaction with high purity elements. The stoichiometric ratios of starting materials were well mixed and pressed into pellets. All the processes were performed under the protection of high-purity Argon due to the air sensitivity of precursors and products. The pellets were sealed in Ta tubes under 0.5 bar of Argon before being sealed into evacuated quartz tubes. The samples were heated at 470 °C for 48 h. Then the products were reground and sintered at 680 °C for 48 h, followed by a quick quenching to room temperature. The recovered samples were characterized by X-ray powder diffraction (XRD) with a Philips X'pert diffractometer using Cu$K\alpha$ radiation. Real compositions of the heavy elements (*i.e.* Cd, Mn and P) were determined by using energy dispersive analysis (EDX) on a commercial Scanning Electron Microscope (SEM). Microstructure was studied by high resolution Transmission Electron Microscope (TEM). The *dc* magnetic properties were examined by using Superconductivity Quantum Interference Device (SQUID, Quantum design), and transport properties were examined by Physical Property Measurement System (PPMS, Quantum design). We calculated the electronic structures by using the density functional theory (DFT) implemented in the code QUANTUM ESPRESSO[36]. The exchange-correlation interactions are described by the Perdew-Burke-Ernzerhof generalized gradients approximation (GGA), and the electronion interactions are represented by the Vanderbilt ultrasoft pseudopotentials.

References

1. Zutic, I., Fabian, J. & Das Sarma, S. Spintronics: Fundamentals and applications. *Reviews of Modern Physics* **76**, 323 (2004).
2. Jungwirth, T. *et al.* Spin-dependent phenomena and device concepts explored in (Ga,Mn)As. *Reviews of Modern Physics* **86**, 855 (2014).
3. Erwin, S. C. & Zutic, I. Tailoring ferromagnetic chalcopyrites. *Nature Materials* **3**, 410 (2004).
4. Ohno, H. Making nonmagnetic semiconductors ferromagnetic. *Science* **281**, 951 (1998).
5. Dunsiger, S. R. *et al.* Spatially homogeneous ferromagnetism of (Ga,Mn)As. *Nature Materials* **9**, 299 (2010).
6. Chen, L. *et al.* Enhancing the Curie temperature of ferromagnetic semiconductor (Ga,Mn)As to 200 K via nanostructure engineering. *Nano Letters* **11**, 2584 (2011).
7. Deng, Z. *et al.* Li(Zn,Mn)As as a new generation ferromagnet based on a I-II-V semiconductor. *Nat Commun* **2**, 422 (2011).
8. Deng, Z. *et al.* Diluted ferromagnetic semiconductor Li(Zn,Mn)P with decoupled charge and spin doping. *Physical Review B* **88**, 081203(R) (2013).
9. Zhao, K. *et al.* New diluted ferromagnetic semiconductor with Curie temperature up to 180 K and isostructural to the '122' iron-based superconductors. *Nat Commun* **4**, 1442 (2013).
10. Zhao, K. *et al.* Ferromagnetism at 230 K in (Ba0.7K0.3)(Zn0.85Mn0.15)2As2 diluted magnetic semiconductor. *Chinese Science Bulletin* **59**, 2524 (2014).
11. Chen, B. J. *et al.* (Sr,Na)(Zn,Mn)2As2: A diluted ferromagnetic semiconductor with the hexagonalCaAl2Si2type structure. *Physical Review B* **90**, 155202 (2014).
12. Zhao, K. *et al.* (Ca,Na)(Zn,Mn)2As2: A new spin and charge doping decoupled diluted ferromagnetic semiconductor. *Journal of Applied Physics* **116**, 163906 (2014).
13. Han, W. *et al.* Diluted ferromagnetic semiconductor (LaCa)(ZnMn)SbO isostructural to "1111" type iron pnictide superconductors. *Science China-Physics, Mechanics and Astronomy* **56**, 2026 (2013).
14. Man, H. *et al.* Ba(Zn(1-2x)MnxCux)2As2: A Bulk Form Diluted Ferromagnetic Semiconductor with Mn and Cu Codoping at Zn Sites. *Sci Rep* **5**, 15507 (2015).

15. Ding, C. *et al*. $(La_{1-x}Ba_x)(Zn_{1-x}Mn_x)AsO$: A two-dimensional 1111-type diluted magnetic semiconductor in bulk form. *Physical Review B* **88**, 041102(R) (2013).
16. Chen, B. *et al*. Structural stability at high pressure, electronic, and magnetic properties of BaFZnAs: A new candidate of host material of diluted magnetic semiconductors. *Chinese Physics B* **25**, 077503 (2016).
17. Hirohata, A. *et al*. Roadmap for Emerging Materials for Spintronic Device Applications. *IEEE Transactions on Magnetics* **51**, 1 (2015).
18. Glasbrenner, J. K., Zutic, I. & Mazin, I. I. Theory of Mn-doped II-II-V semiconductors. *Physical Review B* **90**, 140403(R) (2014).
19. Sun, F. *et al*. Pressure effect on the magnetism of the diluted magnetic semiconductor (Ba1 − xKx)(Zn1 − yMny)2As2 with independent spin and charge doping. *Physical Review B* **93**, 224403 (2016).
20. Sun, F. *et al*. Hole doping and pressure effects on the II-II-V-based diluted magnetic semiconductor (Ba1 − xKx)(Zn1 − yMny)2As2. *Physical Review B* **95**, 094412 (2017).
21. Sun, F. *et al*. Synchrotron X-Ray Diffraction Studies on the New Generation Ferromagnetic Semiconductor Li(Zn,Mn)As under High Pressure. *Chinese Physics Letters* **34**, 067501 (2017).
22. Ning, F. L. *et al*. Suppression of T_C by overdoped Li in the diluted ferromagnetic semiconductor Li1 + y(Zn1 − xMnx)P: A μSR investigation. *Physical Review B* **90**, 085123 (2014).
23. Zhao, G. Q. *et al*. Single Crystal Growth and Spin Polarization Measurements of Diluted Magnetic Semiconductor (BaK)(ZnMn)2As2. *Sci Rep* **7**, 14473 (2017).
24. Wang, R. *et al*. Out-of-plane easy-axis in thin films of diluted magnetic semiconductor Ba1−xKx(Zn1−yMny)2As2. *AIP Advances* **7**, 045017 (2017).
25. Zhao, G. Q. *et al*. Effects of high pressure on the ferromagnetism and in-plane electrical transport of (Ba0.904K0.096)(Zn0.805Mn0.195)2As2 single crystal. *Journal of Physics: Condensed Matter* **30**, 254001 (2018).
26. Suzuki, H. *et al*. Fermi surfaces and p-d hybridization in the diluted magnetic semiconductor Ba1−xKx(Zn1−yMny)2As2 studied by soft x-ray angle-resolved photoemission spectroscopy. *Physical Review B* **92**, 235120 (2015).
27. Frandsen, B. A. *et al*. Local atomic and magnetic structure of dilute magnetic semiconductor(Ba,K)(Zn,Mn)2As2. *Physical Review B* **94**, 094102 (2016).
28. Žutić, I. & Zhou, T. Tailoring Magnetism in Semiconductors. *Science China-Physics Mechanics &. Astronomy* **61**, 067031 (2018).
29. Gu, G. *et al*. Asperomagnetic order in diluted magnetic semiconductor (Ba,Na)(Zn,Mn)2As2. *Applied Physics Letters* **112**, 032402 (2018).
30. Braden, J. G., Parker, J. S., Xiong, P., Chun, S. H. & Samarth, N. Direct Measurement of the Spin Polarization of the Magnetic Semiconductor (Ga,Mn)As. *Physical Review Letters* **91**, 056602 (2003).
31. Bacewicz, R. & Ciszek, T. F. Preparation and characterization of some AIBIICV type semiconductors. *Applied Physics Letters* **52**, 1150 (1988).
32. Shannon, R. D. Revised Effective Ionic Radii and Systematic Studies of Interatomie Distances in Halides and Chaleogenides. *Acta Crystallographica Section A* **A32**, 751 (1976).
33. Coey, J. M., Venkatesan, M. & Fitzgerald, C. B. Donor impurity band exchange in dilute ferromagnetic oxides. *Nat Mater* **4**, 173 (2005).
34. Suzuki, H. *et al*. Photoemission and x-ray absorption studies of the isostructural to Fe-based superconductors diluted magnetic semiconductorBa1−xKx(Zn1−yMny)2As2. *Physical Review B* **91**, 140401(R) (2015).
35. Ohno, H. *et al*. Electric-field control of ferromagnetism. *Nature* **408**, 944 (2000).
36. Giannozzi, P. *et al*. QUANTUM ESPRESSO: a modular and open-source software project for quantum simulations of materials. *Journal of Physics: Condensed Matter* **21**, 395502 (2009).

Acknowledgements

This work is financially supported by National Key R&D Program of China (No. 2017YFB0405703), Ministry of Science and Technology of China (2018YFA03057001, 2015CB921000) & National Natural Science Foundation of China through the research projects (11534016 and 61504166). This work is also supported by the US NSF PIRE (Partnership for International Research and Education: OISE-0968226) and DMR 1105961 projects at Columbia; the JAEA Reimei project at IOP, Columbia. B. Gu is supported by projects with No. Y81Z01A1A9, 110200M208, XDB28000000, 11834014. We thank Prof. Yayu Wang for helpful discussions.

Author Contributions

C.Q.J. conceived & coordinated the research. W.H. conducted the experiments with help of B.J.C. W.H. and Z.D. performed the data analysis. B.G. and S.M. performed the calculations. The obtained results were discussed with G.Q.Z., S.Y., X.C.W., Q.Q.L., W.M.L., J.F.Z., L.P.C., Y.P., X.H.Z., X.S., R.C.Y. and Y.J.U., W.H., Z.D. and C.Q.J. wrote the manuscript. All authors reviewed the manuscript.

Additional Information

Supplementary information accompanies this paper at https://doi.org/10.1038/s41598-019-43754-x.

Competing Interests: The authors declare no competing interests.

Publisher's note: Springer Nature remains neutral with regard to jurisdictional claims in published maps and institutional affiliations.